This is the author's version of an article that has been published in this journal. Changes were made to this version by the publisher prior to publication.
The final version of record is available at http://dx.doi.org/10.1109/TCST.2015.2404893

Phase-Lead Stabilization of Force-Projecting Master-Slave Systems with a New Sliding Mode Filter

Ryo Kikuuwe, *Member, IEEE*, Katsuya Kanaoka, Tomohiro Kumon, and Motoji Yamamoto, *Member, IEEE*

***Abstract*—Force-projecting master-slave control scheme is the reversed implementation of the conventional force-reflecting scheme. This paper presents a method to stabilize force-projecting master-slave systems by using the linear phase-lead compensator and a new nonlinear filter. The nonlinear filter is a modified version of Jin et al.'s (2012) parabolic sliding mode filter, which produces relatively small phase lag. Some numerical properties of the new filter are presented. The filter is then applied to an experimental master-slave system composed of two industrial manipulators. The force scaling factor of 25 was achieved with maintaining the stability.**

***Index Terms*—Master-Slave System, Noise Filter, Force Control, Teleoperation, Sliding Mode**

I. Introduction

Bilateral master-slave (MS) systems[1] have long been studied as one of potential applications of robotics. They extend the utility of human manipulation skills by overcoming barriers of physical distance as well as the difference of scales. For example, robotically-assisted surgery allows humans to perform complex tasks in narrow or small workspaces where human hands cannot work. Another potential application is for heavy-duty robots for work sites such as those of construction and disaster relief.

Studies have been conducted on a variety of control schemes of MS systems. One of the simplest examples is the position-position scheme [1]–[4] (also referred to as a symmetric type [5], [6]), in which the positional difference between the master robot and the slave robot is fed back to the actuator forces in the both sides. In this architecture, the force presented to the operator is influenced by the dynamics of both the master and slave robots. In contrast to this is the force-reflecting scheme (also referred to as a force-position scheme[2]), which employs a force sensor on the slave robot. In this scheme, the force signal is sent to the master robot's actuator, and the slave robot is position-controlled to follow the motion of the master robot. Its advantage is a better transparency, i.e., the force perceived by the operator is not affected by the slave-robot dynamics. The force-reflecting scheme has been investigated since the 1990s [11], [12], and its potential application includes teleoperated surgery [13].

Recently, one of the authors proposed the use of the inverted architecture [14], [15], in which the force sensor is attached to a position-controlled master robot and the force signal is sent to the slave robot's actuators. This control scheme, which we call a *force-projecting* scheme, is intended for heavy-duty applications such as construction and disaster relief, which require the operator's force to be magnified in the slave robot. In such applications, it is reasonable to avoid using slave-side force sensors because they are generally fragile and the external contact may happen at other places than the end-effector. The transparency perceived by the operator is not affected by the master-robot dynamics, but is affected by the slave-robot dynamics. We, however, do not consider it a serious problem by supposing that the operator's perception of the slave-robot dynamics may facilitate a better exploitation of the slave robot's functionality as an extended part of his/her body, though s/he may need a training period to learn the slave robot dynamics. In addition, the direct realization of the operator's force on the slave robot may allow the operator to better exert his/her dynamic motor skills through the slave robot.

This force-projecting MS architecture can be viewed as a special case of the Lawrence architecture [1], [16] and as a sort of "position-force scheme" [7], [8]. Its theoretical properties have been investigated by some researchers [8], [16], but its practical values have not attracted much attention. In applications with a heavy-duty slave robot, the force scaling factor λ (from the master to the slave) should be from 10 to 100 or more and the position scaling factor μ (from the slave to the master) would be, roughly, 0.3 to 1, depending on the dimensions of the master robot. Such high factors have not been considered in the previous studies on the force-reflecting schemes, of which the main application is micromanipulation.

Manuscript received XXX xx, 2014.

The corresponding author is Ryo Kikuuwe (e-mail: kikuuwe@ieee.org, phone: +81-92-802-3174, fax: +81-92-802-0001).

R. Kikuuwe and M. Yamamoto are with the Department of Mechanical Engineering, Kyushu University, 744 Motooka, Nishi-ku, Fukuoka 819-0395, Japan.

K. Kanaoka is with the Advanced Robotics Research Center, Ritsumeikan University, Kusatsu, Japan, and also with Man-Machine Synergy Effectors Inc., Kusatsu, Japan.

T. Kumon was with the Department of Mechanical Engineering, Kyushu University, Fukuoka, Japan, at the time of writing. He is now with KYB Co. Ltd., Tokyo, Japan.

This work was supported in part by Grant-in-Aid for Scientific Research (24360098) from Japan Society for the Promotion of Science (JSPS).

[1]This paper uses the term "master-slave system" to mean a teleoperator that does not always involve significant communication latency. This paper considers master-slave systems that involve no latency.

[2]This paper uses the naming convention with which the information (position or force) received by the operator is mentioned first. This convention has been used by [7]–[9], but some others use the inverted convention [1], [10].

One problem in common to both force-reflecting and force-projecting architectures is that the system can be easily destabilized when the force sensor is constrained by external objects [17], [18]. It has been known that the instability is intensified when the scaling factor λ of the force is set high. The main cause of such instability is that, when the force sensor is elastically constrained by another object, the order of the closed-loop system becomes higher than fourth order, and the poles may move into the right half of the complex plane [12]. The phase lag due to the hardware compliance is also a major cause of the instability [19].

This paper shows the effectiveness of applying phase-lead compensators to the force signal to enhance the stability of the force-projecting MS systems. For reducing the noise produced by the differentiator in the phase-lead compensators, this paper presents a modified version of a parabolic sliding mode filter (PSMF) [20], [21], which is a recently-proposed noise reduction filter that produces relatively small phase lag [21]. The presented controller, composed of the sliding mode filter and the phase-lead compensator, is validated by using an experimental MS system comprising two industrial manipulators. It achieved the force scaling factor of $\lambda = 25$ with the position scaling factor of $\mu = 1$.

The rest of this paper is organized as follows. Section II formulates asymmetric MS control schemes without time delay, which can be either of the force-reflecting and force-projecting type. This section also discusses related study and the theoretical necessity of phase-lead compensation for position and/or force signals. Section III presents a new sliding mode filter for reducing the noise, which would be contained in the phase-led signals. Section IV shows experimental results to show the effectiveness of the combination of the proposed filter and the phase-lead compensation applied to the force signal. Section V provides concluding remarks.

II. Force-Projecting/Reflecting MS Systems

A. Instability and Phase Lag

The control architecture of a force-reflecting/projecting MS system is shown in Fig. 1. In the force-reflecting scheme, the slave robot is equipped with a force sensor and is position-controlled, and thus it can be viewed as an admittance-type robot. In contrast, the master robot needs to be backdrivable (i.e., an external force needs to influence the measured position) and is torque-commanded, and thus it can be viewed as an impedance-type robot. A force-projecting MS system [14], [15] has the reversed architecture, in which the master robot is of the admittance type and the slave robot is of the impedance type. In order to discuss these two types in a unified framework, this paper uses the terms "admittance robot" and "impedance robot" to mean either robot of the force-reflecting and force-projecting MS systems. The force measured by the force sensor on the admittance robot is produced by the actuators of the impedance robot. The position of the impedance robot is used as the desired position command provided to the admittance robot.

For simplicity, the discussion in this section is restricted to the one-dimensional case with no communication latency.

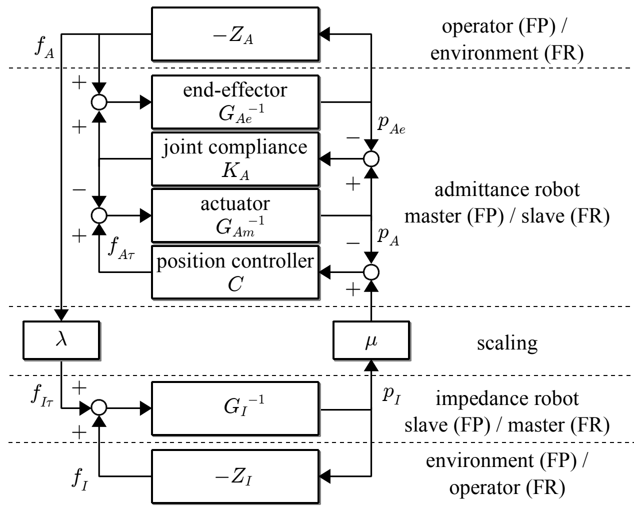

Fig. 1. Basic control architecture of a force-projecting (FP) or force-reflecting (FR) MS system.

Hereafter, all symbols are defined in the Laplace transform domain and are functions of the Laplace operator $s \in \mathbb{C}$. The subscripts I and A represent the impedance and admittance robots, respectively. Now, we describe the dynamics of the impedance robot as follows:

$$G_I p_I = f_{I\tau} + f_I \tag{1}$$

where p_I and G_I are the position and the dynamics of the impedance robot, respectively. Here we are assuming that two forces are acting on the robot: the actuator force $f_{I\tau}$ and an external force f_I.

We consider an admittance robot that has compliance in its joint and/or link between the actuator and the end-effector. Then, its dynamics can be described as follows:

$$G_{Am} p_A = f_{A\tau} + K_A(p_{Ae} - p_A) \tag{2}$$

$$G_{Ae} p_{Ae} = f_A + K_A(p_A - p_{Ae}). \tag{3}$$

Here, p_A and p_{Ae} are positions of the actuator and the end-effector, respectively. The symbols G_{Am} and G_{Ae} denote the dynamics of the actuator and the end-effector, respectively. They are connected by the compliance K_A, which is a transfer function if there is damping. The expressions (2)(3) can be rewritten as follows:

$$G_A p_A = f_{A\tau} + U_A f_A \tag{4}$$

$$p_{Ae} = U_A p_A + \frac{f_A}{K_A + G_{Ae}} \tag{5}$$

where

$$G_A \triangleq \frac{G_{Ae} + G_{Am} + G_{Ae} G_{Am}/K_A}{1 + G_{Ae}/K_A} \tag{6}$$

$$U_A \triangleq \frac{K_A}{K_A + G_{Ae}}. \tag{7}$$

In the extreme case of the rigid admittance robot where $|K_A| = \infty$, we have $U_A = 1$, $p_A = p_{Ae}$, and $G_A = G_{Am} + G_{Ae}$. Here, we assume that p_A is measured by the position sensor and f_A is measured by a force sensor.

We consider the following control law:

$$f_{I\tau} = \lambda f_A \tag{8}$$
$$f_{A\tau} = C(\mu p_I - p_A) \tag{9}$$

where C denotes the transfer function of a position controller. This is a standard form of force-reflecting scheme when the admittance robot is used as the slave robot. The position and force scaling factors are denoted by μ and λ, respectively, following the naming convention in the literature [12], [17], [19]. In force-reflecting MS systems, μ is determined by the geometric requirements imposed by the application, and λ is determined so that the reflected force is large enough to be perceived by the operator.

The contact to external objects (the environment in the work space or the human operator) can be described as follows:

$$f_A = -Z_A p_{Ae} \tag{10}$$
$$f_I = -Z_I p_I \tag{11}$$

where Z_A and Z_I are the impedance representations of the dynamics of the external objects. If the impedance robot has the compliance between its end-effector and its motor, it may be included in the transfer function Z_I.

By eliminating p_A and $f_{A\tau}$ from (4), (5) and (9), one can obtain the following:

$$p_{Ae} = \mu U_C U_A p_I + f_A/G_{AL} \tag{12}$$

where

$$U_C \triangleq \frac{C}{G_A + C} \tag{13}$$
$$G_{AL} \triangleq G_{Ae} + \frac{(G_{Am} + C)K_A}{G_{Am} + C + K_A}. \tag{14}$$

Fig. 2 shows a block diagram including U_C and G_{AL}, which is equivalent to the one in Fig. 1. Here, U_C can be interpreted as a phase-lag effect caused by the position controller, and G_{AL} as a local dynamics of the position-controlled admittance robot. In the extreme case of the perfect position control and the rigid admittance robot (i.e., $|C| = \infty$ and $|K_A| = \infty$), one obtains $U_A = U_C = 1$ and $|G_{AL}| = \infty$, which implies that $p_A = p_{Ae}$. If K_A is a simple viscoelasticity represented by a first-order polynomial, if the actuator G_{Am} is a simple mass represented by a second-order polynomial, and if the controller C is a PD or PID controller chosen so that $(G_{Am} + C)^{-1}$ is stable, then one can easily see that the denominator of G_{AL} is stable, and thus it cannot be a source of instability.

Considering (1), (8), and (11), one can obtain the open-loop relation from f_A to p_{Ae} as follows:

$$p_{Ae} = G_S f_A \tag{15}$$

where

$$G_S \triangleq \frac{\lambda\mu U_C U_A}{G_I + Z_I} + \frac{1}{G_{AL}}. \tag{16}$$

In the case of force-projecting scheme, the transfer function G_S is the admittance of the system felt by the operator. If the position control is perfect and the admittance robot is rigid (i.e., $U_C U_A = 1$ and $|G_{AL}| = \infty$), the best transparency is achieved, i.e., the operator feels only the combined dynamics of the environment and the slave robot scaled by the factor of $\lambda\mu$.

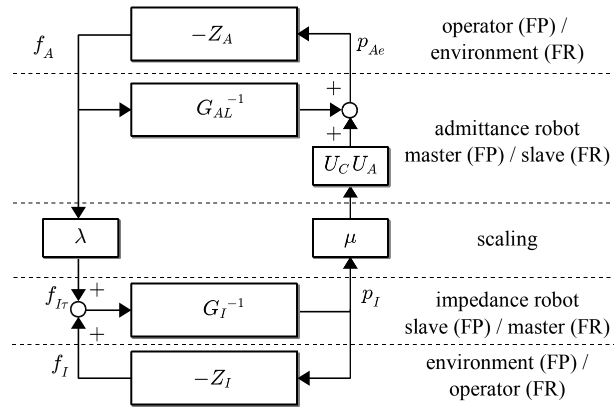

Fig. 2. Simplified equivalent block diagram of Fig. 1.

The open-loop system (16) is closed by the feedback (10), and $|Z_A|$ can be high during firm grasping by the operator in the force-projecting scheme, or during contact with stiff environment in the force-reflecting scheme. Such situations can result in instability if there is a frequency range at which $\angle G_S \leq -\pi$. Considering the expression (16), one can see that the phase-lag blocks U_C and U_A can be sources of the instability, and that the instability may be avoided by inserting appropriate compensators at the places of λ and μ. To be more specific, the inserted compensators should lead the phase or reduce the gain at the high frequency range where $\angle G_S \leq -\pi$. Thus, one can conclude that appropriate low-pass filtering and phase-lead compensation should be performed at either or both of the places of λ and μ.

B. Related Work

There have been many works analyzing stability properties of MS systems illustrated in Fig. 1. The latency in the communication channel has been a primary concern in the field of *tele*-operation. This paper, however, does not consider it any further because there are many imaginable applications of MS systems with negligible communication latency, especially those with position/force scaling. Even in such applications, the phase-lag blocks U_C and U_A in (16) may destabilize the system. One imaginable approach to suppress the instability is to enhance the passivity by, for example, adding damping to either side of the system [22]. It however can result in deteriorated transparency and additional fatigue of the operator. Another approach is a shared compliant control [23], [24], which employs a local force feedback in the admittance robot. In the framework of Fig. 2, its effect can be interpreted to be an enhancement of the block G_{AL}^{-1}, and thus it can also deteriorate the transparency.

To compensate the phase lag caused by $U_C U_A$, it would be logical to use a phase-lead compensator, which involves a derivative action. The use of force rate has been reported in regard to force control [25]–[27], but it has been recognized that the noise amplified by the differentiation needs to be suppressed. For example, Qian and De Schutter [25] used a low-pass filter with a cutoff frequency of 30 Hz, and Xu et al. [26] used only the sign information of the force rate. Effects of low-pass filters in the force-reflecting scheme have also been investigated. Daniel and McAree [12, Sec. 4.2] suggested that low-pass filters improve the stability under some assumptions such as $\lambda\mu < 1$ and infinite environment stiffness. In contrast, Willaert et al. [19] reported negative effects of low-pass filters by showing that the critical environment stiffness decreases as the cutoff frequency decreases. Such contradiction can be attributed to two effects of low-pass filters, which increase the gain margin (i.e., reduce the gain in high-frequency range) but decrease the phase margin (i.e., increase the phase lag).

The open-loop transfer function G_S in (16) also suggests that the gain margin is reduced when the scaling factors λ and μ are increased. The values of the factor $\lambda\mu$ considered in the literature are not so high. In fact, many studies, such as [12], [28], restrict their analysis or experiments to the case of $\lambda\mu < 1$. For micromanipulation under a time delay of 1 s, Boukhnifer and Ferreira [28] used the values of $\lambda\mu < 1.4$. Higher values found in the literature are, for example, $\lambda\mu = 5.17$ [19] and $\lambda\mu = 10$ [17].

There are some MS control schemes that are different from but similar to the scheme illustrated in Fig. 1. Variations exist mainly in the local controller of each of the master and slave robots. For example, some control schemes [29]–[31] similar to the force-reflecting scheme employ a local admittance controller to regulate the force on the master robot's end-effector. Specifically, in the "pseudo-admittance" control [29], the master robot of the impedance type is locally controlled with admittance control and the external force measured at the slave robot is directly superposed to the master robot's actuator force. Some other schemes [9], [10], [32] are similar to the force-projecting scheme in the sense that the force information is sent from the master side to the slave side. In these schemes, however, the slave robot is also equipped with a force sensor, and the operator's force is intended to be matched with the slave robot's end-effector force, not with the actuator force. Optimization of the transparency employing the slave-side force sensor has also been studied [9]. In applications where hard collisions or off-sensor contacts may occur, however, the use of the slave-side force sensor should be avoided.

III. Nonlinear Filters with Smaller Phase Lag

The previous section showed that a major source of instability of the force-reflecting and force-projecting MS systems is the phase lag caused by the compliance of the position controller and the admittance robot. It has been shown that a phase-lead compensator would be effective but it demands derivative actions on the position and/or force signals, which amplify the noise in the signals. Thus, it is logical to suppose that a noise-reduction filter that results in relatively small phase lag would be necessary to be combined with a phase-lead compensator.

This section presents a new noise-reduction filter that produces smaller phase lag than linear filters do. The new filter is a modified version of Jin et al.'s [20], [21] sliding mode filter.

A. Jin et al.'s Parabolic Sliding Mode Filter (J-PSMF)

Jin et al.'s Parabolic Sliding Mode Filter (hereafter, J-PSMF) [20], [21], which has been proposed by the authors' group, is a noise reduction filter based on sliding mode. It has been reported that its frequency-gain characteristics are similar to those of the second-order linear low-pass filter but produces smaller phase lag [21]. The effectiveness of the filter has been supported by experiments in which an admittance-controlled robot was stabilized by the use of J-PSMF and a phase-lead compensator [21] and by the use of J-PSMF and acceleration feedforward [33].

The continuous-time representation of J-PSMF is given as follows:[3]

$$\dot{x}_1 = x_2 \tag{17a}$$
$$\dot{x}_2 \in -\frac{H+1}{2}F\,\mathrm{sgn}(\sigma) - \frac{H-1}{2}F\,\mathrm{sgn}(x_2) \tag{17b}$$
$$y = x_1 \tag{17c}$$

where

$$\sigma \triangleq x_2 + \mathrm{sgn}(x_1 - u)\sqrt{2F|x_1 - u|} \tag{18}$$
$$\mathrm{sgn}(x) \triangleq \begin{cases} x/|x| & \text{if } x \neq 0 \\ [-1, 1] & \text{if } x = 0. \end{cases} \tag{19}$$

Here, u and y are the input and the output of the filter, respectively, and $H > 1$ and $F > 0$ are parameters appropriately chosen. The magnitude of $\ddot{y} = \dot{x}_2$ is bounded by HF. This filter has two sliding surfaces: $\sigma = 0$ and $x_2 = 0$.

It may be worth noticing that the state-space representation (17) is equivalent to that of a system consisting of a unit mass subject to Coulomb friction and a bang-bang controller. In addition, setting $H = 1$ in (17) reduces it into the filter presented by Emaru and Tsuchiya [37] and Han and Wang [38].

The previous papers [20], [21] have also presented a discrete-time algorithm of the filter (17), which is based on the backward (implicit) Euler discretization. Through the derivation detailed in [20], its discrete-time algorithm can be obtained as follows:[4]

$$x_M := FT\,\Phi\left(\frac{u(k) - x_1(k-1)}{FT^2}\right) \tag{20a}$$
$$x_L := \mathrm{clip}(x_2(k-1) + [-HFT, -FT], 0) \tag{20b}$$
$$x_U := \mathrm{clip}(x_2(k-1) + [FT, HFT], 0) \tag{20c}$$
$$x_2(k) := \mathrm{clip}([x_L, x_U], x_M) \tag{20d}$$
$$x_1(k) := x_1(k-1) + Tx_2(k) \tag{20e}$$

[3]Mathematical expressions like (17b), which involve the symbol "$\in$" and derivatives, are referred to as differential *inclusions* [34] instead of differential equations. The expression (17b) is different from the one originally presented in [20], [21], but they are equivalent to each other as detailed in [35]. Moreover, the definition of σ has been modified from $\sigma \triangleq 2F(x_1 - u) + |x_2|x_2$ to (18), to highlight the similarity to a second-order sliding mode controller in the literature, e.g., eq.(14) in [36]. This modification does not alter the definition (17) of the filter because it does not alter $\mathrm{sgn}(\sigma)$.

[4]This paper employs the notation in which $x + [y, z]$ means $[x + y, x + z]$ where $x, y, z \in \mathbb{R}$. This notation is consistent with the one that has often been used in the literature, e.g., [34].

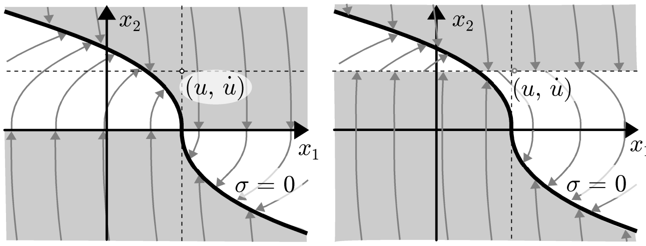

(a) Jin et al.'s PSMF (b) modified PSMF

Fig. 3. State-space illustrations of (a) J-PSMF (17) and (b) M-PSMF (23). The magnitude of $\dot{x}_2$ is F in the white regions and HF in the gray regions.

where

$$\Phi(x) \triangleq \mathrm{sgn}(x)\left(\sqrt{1+2|x|}-1\right) \tag{21}$$

$$\mathrm{clip}([a,b],x) \triangleq \begin{cases} b & \text{if } x > b \\ x & \text{if } x \in [a,b] \\ a & \text{if } x < a. \end{cases} \tag{22}$$

Due to the use of the implicit Euler integration method, the obtained algorithm (20) is free from discontinuous functions. Thus, the chattering, which is a common problem of sliding mode techniques, does not happen around the sliding surfaces $\sigma = 0$ and $x_2 = 0$.

The stability properties of the filter (17) have been investigated in a previous paper [35], but the analysis is restricted to the case where $\dot{u} = 0$. A flaw of the filter (17) is that, when $\dot{u} \neq 0$, the sliding mode at the surface $x_2 = 0$ cannot be realized.

B. Modified PSMF (M-PSMF)

This paper considers the following modified version of PSMF, which we hereafter call M-PSMF:

$$\dot{x}_1 = x_2 \tag{23a}$$
$$\dot{x}_2 \in -\frac{H+1}{2}F\mathrm{sgn}(\sigma) - \frac{H-1}{2}F\mathrm{sgn}(x_2 - \dot{u}) \tag{23b}$$
$$y = x_1. \tag{23c}$$

Fig. 3 illustrates the difference between J-PSMF (17) and M-PSMF (23). The filter (23) possesses the following property, of which the proof is provided in the appendix:

Theorem 1. *With the system (23), assume that there exist positive scalars P and Q with which the following condition is satisfied for all $t > t_0$:*

$$|\dot{u}| < P \wedge |\ddot{u}| < Q < \min\left((H-1)F/2, F\right). \tag{24}$$

Then, there exists a $t_1 > t_0$ with which the following is satisfied:

$$\forall t > t_1,\ \sigma = 0 \wedge |x_2 - \dot{u}| \leq \frac{PQ}{F-Q}. \tag{25}$$

This theorem implies that, a ramp input ($Q = 0$) with $|\dot{u}| < P$ to the filter results in $\sigma \to 0$ and $x_2 \to \dot{u}$, which leads to $y \to u - |\dot{u}|\dot{u}/(2F)$. That is, the filter output y exhibits a steady-state error under a ramp input, as the so-called "type-1" systems do in the linear control theory. This property is not considered problematic in applications to force signals because, in practical situations, monotonic increase or decrease does not last long in such signals.

In a similar manner to the case of J-PSMF, a discrete-time algorithm of M-PSMF (23) can be obtained as follows:

$$x_M := FT\,\Phi\left(\frac{u(k) - x_1(k-1)}{FT^2}\right) \tag{26a}$$
$$w := (u(k) - u(k-1))/T \tag{26b}$$
$$x_L := \mathrm{clip}(x_2(k-1) + [-HFT, -FT], w) \tag{26c}$$
$$x_U := \mathrm{clip}(x_2(k-1) + [FT, HFT], w) \tag{26d}$$
$$x_2(k) := \mathrm{clip}([x_L, x_U], x_M) \tag{26e}$$
$$x_1(k) := x_1(k-1) + Tx_2(k). \tag{26f}$$

Again, it should be noted that the chattering does not happen in this algorithm because it does not include discontinuous functions.

C. Frequency-Domain Analysis of M-PSMF

Some numerical results are now presented to show properties of J-PSMF and M-PSMF. Sinusoidal inputs $u(t) = A_u \sin(2\pi f_u t)$ were provided to the filters, and the amplitude and phase of the corresponding frequency component of the output $y(t)$ were recorded. For comparison, first- and second-order linear low-pass filters (1-LPF and 2-LPF, respectively) were also used. The LPFs were implemented with the bilinear transform and the 2-LPF was a Butterworth filter.

The results are shown in Fig. 4. One can see that M-PSMF exhibits a similar response to that of the 1-LPF, but its phase lag is smaller than that of 1-LPF. This is in contrast to J-PSMF, of which the gain characteristics are close to but the phase lag is smaller than 2-LPF. Fig. 4(b) and (c) show the influence of the parameter H. With J-PSMF, the effect of H is almost saturated at $H = 10$. This result is consistent with results in a previous report, e.g., [21, Fig.5]. With M-PSMF, in contrast, the phase lag decreases as H increases until $H = 50$.

One important feature common to J-PSMF and M-PSMF is that, due to their nonlinearities, the output amplitude is not proportional to the input amplitude at each frequency. Fig. 5 shows the results obtained by various input amplitudes. One can see that the cross-over frequency in the amplitude plot depends on the input amplitude A_u. This means that, when one intends to use J-PSMF or M-PSMF, a "cut-off frequency" cannot be explicitly specified.

D. Limitation of the Frequency-Domain Analysis

It should be cautioned that, with a general input signal $u(t)$ containing many frequency components, each frequency component of the output $y(t)$ may be influenced by other frequency components of the input $u(t)$. This means that the frequency-response characteristics of the filters do not capture the whole property of the filters.

Based on frequency-domain analysis such as the describing function method, some other nonlinear filters can also be viewed as low-pass filters with reduced phase shifts. One example [39, p.188] is the filter illustrated in Fig. 6, which is a serial combination of a low-pass filter, a saturation block

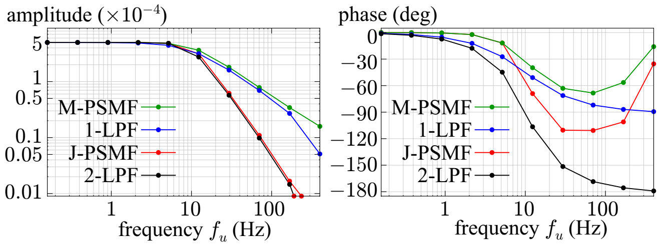

(a) M-PSMF (H=100), J-PSMF (H=10), and LPFs

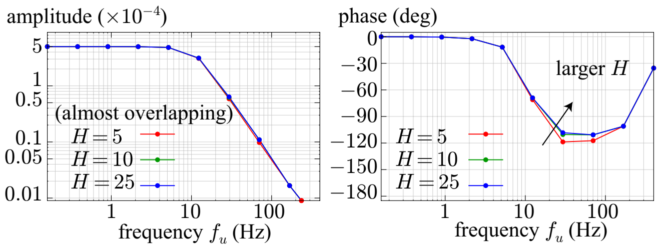

(b) J-PSMF (H=5, 10, 25)

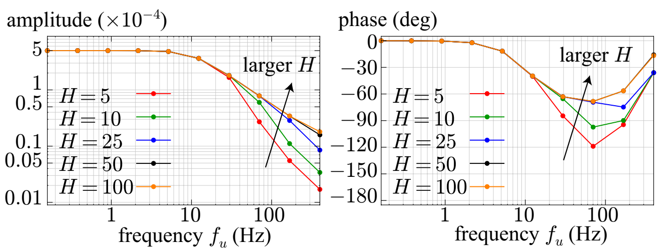

(c) M-PSMF (H=5, 10, 25, 50, 100)

Fig. 4. Frequency response of PSMFs ($F = 1$ s^{-2}) and LPFs (cut-off frequency: 10 Hz). The input amplitude was $A_u = 5\times10^{-4}$ and the timestep size was $T = 0.001$ s.

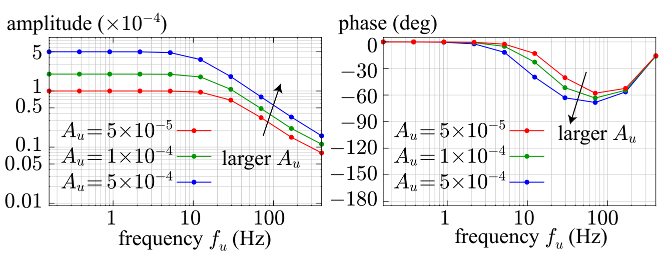

Fig. 5. Frequency response of M-PSMF ($F = 1$ s^{-2}, $H = 50$) against various amplitudes A_u of sinusoidal inputs u. The timestep size was $T = 0.001$ s.

and a high-pass filter. It can be viewed as a low-pass filter with no phase shift when a single sinusoidal input is provided. However, when the input signal contains low- and high-frequency components, its output is not practically useful, as illustrated with the numerical examples in Fig. 7(a)(b). In contrast, Fig. 7(c) clearly shows that the M-PSMF better preserves the low-frequency component under the existence of high-frequency component. More complete analysis to explain time-domain characteristics of M-PSMF is left open for future study.

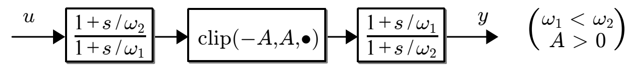

Fig. 6. A nonlinear filter that can be viewed as a low-pass filter without phase lag according to the describing function method (adopted from Fig. 5.31 of [39]).

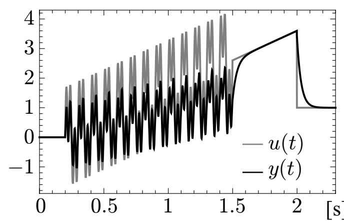

(a)

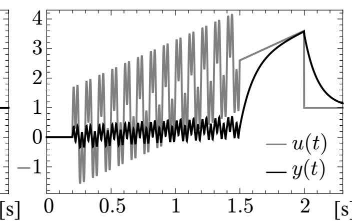

(b)

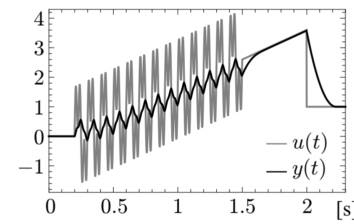

(c)

Fig. 7. Examples of time-domain response of filters to a common input signal $u(t)$. (a)(b) The filter of Fig. 6 with $\{\omega_1, \omega_2, A\} = \{5$ rad/s, 400 rad/s, $4\}$ and $\{1.5$ rad/s, 400 rad/s, $4\}$, respectively. (c) M-PSMF with $\{F, H\} = \{100$ s$^{-2}, 300\}$.

IV. Experiments

A. Setup

The proposed sliding mode filter combined with a phase-lead compensator was tested by using an experimental force-projecting MS system shown in Fig. 8. The system was composed of two 6-DOF industrial manipulators, MOTOMAN-HP3J and MOTOMAN-UPJ (Yaskawa Electric Corporation), which had identical kinematic structure to each other. The robots were controlled with a PC running the ART-Linux operating system. The sampling interval of the controller was $T = 0.001$ s. Each robot had six AC servomotors integrated with harmonic-drive transmissions and optical encoders. A six-axis force sensor (Nitta Corporation) was attached on the tip of the MOTOMAN-HP3J, which was used as the admittance robot. As can be seen in Fig. 8(a), a grip was attached to the force sensor.

Only the force-projecting scheme was tested because, if the system is used as a force-reflecting MS system, the safety of the experimenter and the protection of the force sensor cannot be guaranteed. In the force-reflecting scheme with $\lambda > 1$, the admittance robot gains contact with an external object through the force sensor, and the contact force on the force sensor is magnified at the actuator of the impedance robot, which is held by the experimenter. Manipulators that are so powerful as to damage humans or force sensors are not suited for such applications.

Fig. 9 shows a block diagram of the experimental setup. In the controller, the force vector $\boldsymbol{f}_A \in \mathbb{R}^6$ (composed of a translational force vector and a moment vector) on the

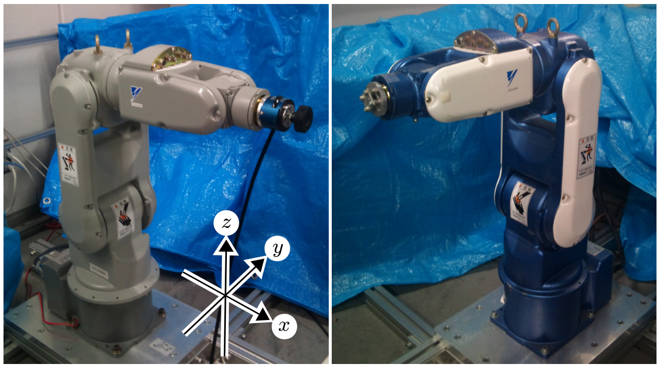

(a) MOTOMAN-HP3J: master (admittance) robot

(b) MOTOMAN-UPJ: slave (impedance) robot

Fig. 8. Experimental force-projecting MS system

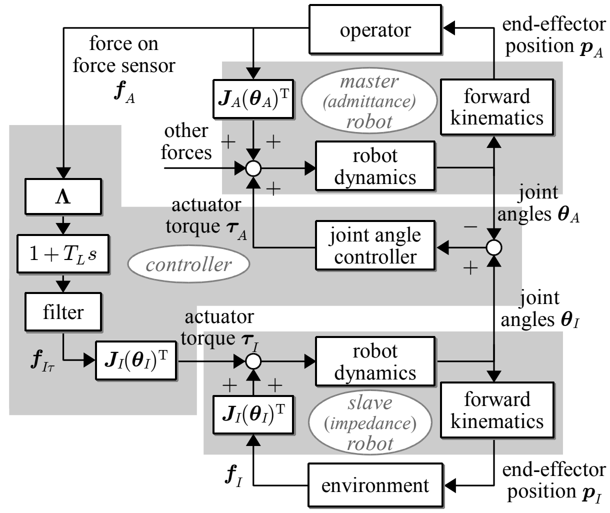

Fig. 9. Block diagram of the experimental force-projecting MS system. Here, $\boldsymbol{\Lambda}$ is for scaling the translational components, being defined as $\boldsymbol{\Lambda} \triangleq \mathrm{diag}[\lambda, \lambda, \lambda, 1, 1, 1]$, and $\boldsymbol{J}_A(\boldsymbol{\theta}_A)$ and $\boldsymbol{J}_I(\boldsymbol{\theta}_I)$ are the Jacobian matrices of the master and the slave robots, respectively.

master robot was measured by the force sensor. Only the three translational entries of $\boldsymbol{f}_A$ were scaled by the factor of λ $(\in \{8, 15, 25\})$.[5] Then, each of the six entries of the force signal was passed through a phase-lead compensator described as follows:

$$G(s) = 1 + T_L s, \tag{27}$$

which was implemented by using the Euler method, i.e., $s := (1-z^{-1})/T$. Here, T_L was chosen as $T_L \in \{0\text{ s}, 0.02\text{ s}\}$ to exhibit the difference caused by the presence of the phase-lead compensator. The value 0.02 s was chosen through preliminary experiments to exhibit the best performance considering the trade-off between its effects of noise amplification and stabilization. The obtained signal was fed to one of the noise-reduction filters listed below:

- **NF:** No filtering
- **1-LPF:** $G_{F1}(s) = 2\pi f_c/(s + 2\pi f_c)$
- **2-LPF:** $G_{F2}(s) = (2\pi f_c)^2/(s^2 + \sqrt{2}(2\pi f_c)s + (2\pi f_c)^2)$
- **J-PSMF:** the algorithm (20)
- **M-PSMF:** the algorithm (26).

Here, f_c is the cut-off frequency of LPFs in herz, and the LPFs were implemented by using the bilinear transform,[6]i.e., $s := 2(1 - z^{-1})/(T(1 + z^{-1}))$. It should be noted that the phase-lead compensator (27) combined with a 1-LPF forms a linear phase-lead-lag compensator.

Other filtering methods were not compared in this experiment. For example, we cannot deny the possibility that some model-based filters, such as Kalman filters, may outperform the PSMFs if an elaborate physical model of the master-robot compliance is taken into account. In contrast to such model-based filters, PSMFs are simple, involving only two design parameters, F and H. Thus, we leave such comparison outside the scope of this paper. Other classes of force-reflecting control schemes were not compared either. It is because most of previous methods are either targeted to the significant time-delay [40], dependent on the robots' dynamics models [13], or specific to the case with the impedance robot being grabbed by a human operator [41].

As shown in Fig. 9, the application of the scaling, the phase-lead compensation and the filtering to the force signal $\boldsymbol{f}_A$ yields the signal $\boldsymbol{f}_{I\tau} \in \mathbb{R}^6$. It was then multiplied by the transpose of the slave robot's Jacobian matrix $\boldsymbol{J}_I(\boldsymbol{\theta}_I) \in \mathbb{R}^{6\times 6}$, which is a function of the slave robot's joint angles $\boldsymbol{\theta}_I \in \mathbb{R}^6$, to obtain its statically equivalent joint torque $\boldsymbol{\tau}_I \in \mathbb{R}^6$, which was used as the torque command to the slave robot. The angle of each joint of the master robot was controlled to track the angle of the correspondent joint of the slave robot. That is, the position scaling factor was set as $\mu = 1$. Each joint was controlled by using a sliding-mode-like position controller presented in [33], which is equivalent to the ordinary PID controller when the actuator torques are not saturated. The gains of these controllers were chosen to realize as stiff position control as possible.

As can be seen in Fig. 9, the phase-lead compensator $1 + T_L s$ was used only for the force signal and was not used for the position signal. We tried some preliminary experiments in which phase-lead compensation was applied to the position signal. We however did not observe any apparent improvements, and found that it resulted in high-frequency vibration in the system when T_L was large and the filtering was insufficient. At this time, there is no definitive explanation on this observation. One possibility is that it is because the high-frequency components of the position signal were corrupted due to the limited resolution of the optical encoders and the elasticity of the joints.

In the graphs in this section (Fig. 10 and later), $f_{I\tau y}$ denotes the y-translational component of $\boldsymbol{f}_{I\tau}$ in Fig. 9. Here, note that the coordinate system is defined in Fig. 8(a). The same rule applies to f_{Ay} and p_{Ay}, which are the y-translational

[5]When the rotational entries were also magnified by λ, the three joints closest to the end-effector became excessively sensitive to the moment applied from the experimenter, and it became difficult to operate as intended. Further investigation may be needed to circumvent this problem, which may involve the geometrical design of the grip of the master robot.

[6]The bilinear transform was used for LPFs for better consistency with the frequency analysis in Fig. 4. On the other hand, Euler discretization was used for the phase lead compensator (27) because it excessively magnifies the high-frequency components when it is implemented with the bilinear transform.

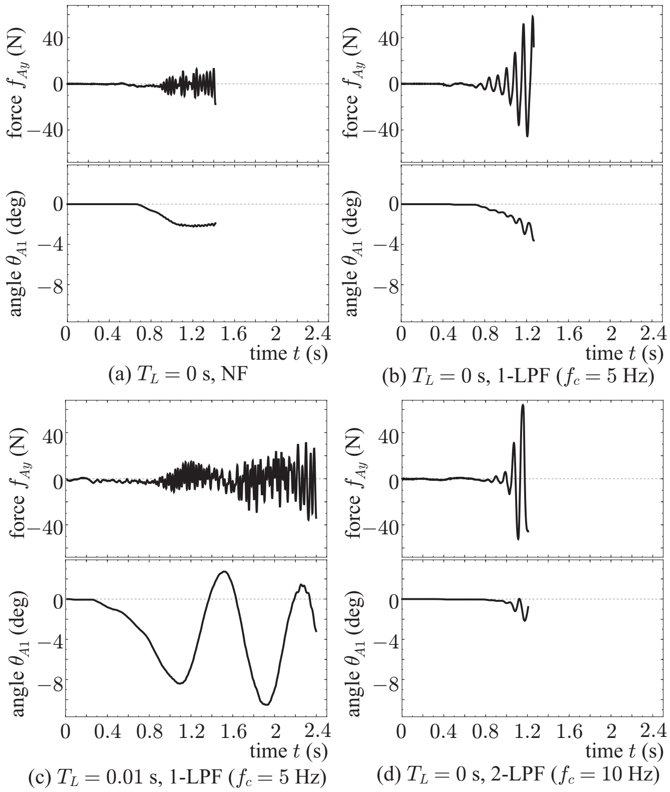

Fig. 10. Experiment I: the master robot's end-effector was grasped and was moved if possible. The force scaling factor was $\lambda = 8$. In (a)(b)(d), the system went unstable before it was moved by hand. In (c), it was rather stable and can be moved by hand for a certain period of time, but it eventually went unstable.

components of $\boldsymbol{f}_A$ and $\boldsymbol{p}_A \in \mathbb{R}^6$, respectively. The symbol θ_{A1} is the angle of the first (base) joint of the master robot, which is the first component of $\boldsymbol{\theta}_A \in \mathbb{R}^6$.

B. Experiment I: 1-DOF Motion with Linear Filters

A set of experiments was performed to exhibit the limitation of the linear filters combined with the phase-lead compensator. For safety reasons, in these experiments, the five joints except the base joint of the slave robot were locked by local position controllers with as high gains as possible. As a result, the end-effectors of the both robots were allowed to move only horizontally along circular paths, maintaining the configurations seen in Fig. 8. The experimenter firmly grasped the master robot's end-effector and tried to move it horizontally.

The force scaling factor was fixed at $\lambda = 8$ and the following filters were used:

- NF
- 1-LPF with $f_c = 5$, 10, and 20 Hz
- 2-LPF with $f_c = 5$, 10, and 20 Hz.

The coefficient T_L of the phase-lead compensator was chosen as $T_L = 0$ or 0.02 s. It should be noted that, when $2\pi T_L f_c < 1$, a LPF combined with the phase-lead compensator $1 + T_L s$ produces a phase-lag effect. It was however included in the experiments for comparison.

The result was that all the combinations resulted in instability or vibration, which sometimes led to the emergency stop of the servo amplifiers of the actuators. Fig. 10 shows some of the results. The details are as follows:

- **NF**: When $T_L = 0$, a firm grasping resulted in vibratory, unstable behavior as shown in Fig. 10(a). Setting $T_L > 0$ produced strong noisy sound from the actuators, which can be attributed to the magnified noise in the force signal.
- **1-LPF**: Also in this case, when $T_L = 0$, firm grasping resulted in vibratory, unstable behavior as shown in Fig. 10(b), where the frequency of the oscillation was dependent on the cut-off frequency f_c. Setting $T_L > 0$ increased the noisy sound from the actuators but slightly improved the stability especially when $2\pi T_L f_c < 1$. The most stable combination was $f_c = 5$ Hz and $T_L = 0.01$ s, with which the experimenter was able to move the end-effector by hand for a certain period of time, as shown in Fig. 10(c), but it eventually went unstable.
- **2-LPF**: All combinations of f_c and T_L resulted in instability, as shown in Fig. 10(d).

These results imply that, the linear filters cannot be used in practice with higher values of λ. Thus, in the rest of this section, the linear filters are not taken into consideration any further.

C. Experiment II: 1-DOF Motion with PSMFs

Next, the effects of J-PSMF and M-PSMF combined with phase-lead compensation were investigated. In these experiments, the five joints were locked as were in Experiment I. The force scaling factor was chosen as $\lambda = 15$. The experimenter grasped the master robot's end-effector and intended to produce reciprocal horizontal motion at the frequency of 3 Hz, being paced by a metronome. The parameters of the PSMFs (H and F) were chosen through preliminary experiments so that they produce good results without excessively affected by the noise in the force signal. The H value used here ($H = 300$) is not consistent with the results of the frequency-domain analysis presented in section III-C, in which the effect of H saturates at $H = 50$, but we observed distinct performance differences in $H > 100$ in this experimental setup. We leave this discrepancy for future study.

For the purpose of evaluation, we used the following quantity:

$$w \triangleq \boldsymbol{f}_A{}^T \boldsymbol{v}_A, \tag{28}$$

which can be interpreted as the power exerted by the operator on the master robot. Here, $\boldsymbol{v}_A \in \mathbb{R}^6$ is the velocity vector of the end-effector of the master robot, which is composed of a 3-dimensional translational velocity vector and a 3-dimensional angular velocity vector. When w tends to be negative, one can say that it is an undesirable situation because the passivity of the system is being lost.

The results are shown in Fig. 11. When $T_L = 0$, it was difficult to continue the periodic movement due to irregular resistive forces from the master robot. One can see that the supply rate w in Fig. 11(a)(b)(c) has negative values of large magnitude, which mean that, roughly speaking, the master robot's motion was not the motion intended by the

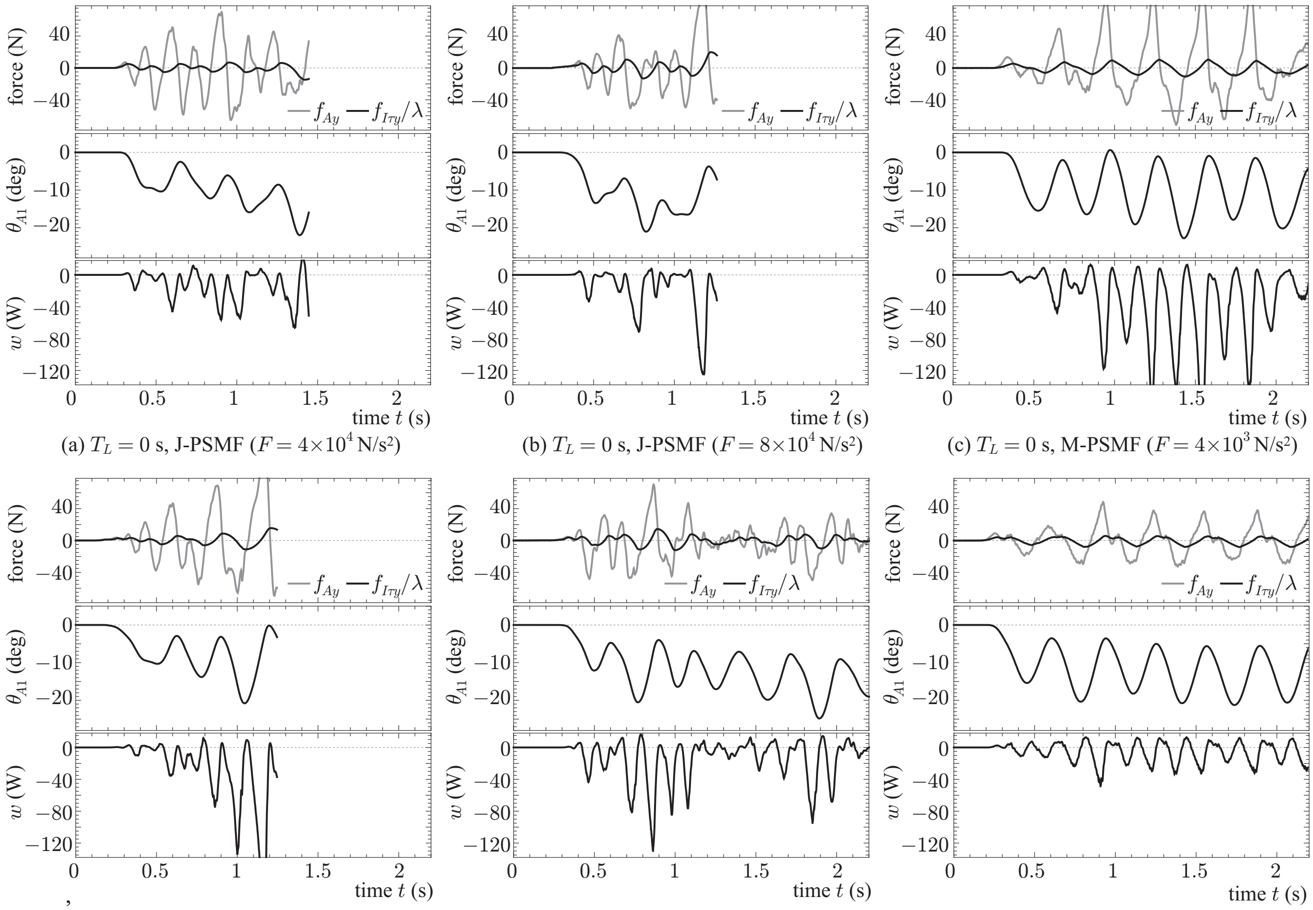

(a) $T_L = 0$ s, J-PSMF ($F = 4{\times}10^4$ N/s²)
(b) $T_L = 0$ s, J-PSMF ($F = 8{\times}10^4$ N/s²)
(c) $T_L = 0$ s, M-PSMF ($F = 4{\times}10^3$ N/s²)
(d) $T_L = 0.02$ s, J-PSMF ($F = 4{\times}10^4$ N/s²)
(e) $T_L = 0.02$ s, J-PSMF ($F = 8{\times}10^4$ N/s²)
(f) $T_L = 0.02$ s, M-PSMF ($F = 4{\times}10^3$ N/s²)

Fig. 11. Experiment II: the master robot's end-effector was grasped and was intended to be moved at the frequency of approximately 3 Hz. The force scaling factor was $\lambda = 15$. The H-values were $H = 5$ with J-PSMF and $H = 300$ with M-PSMF. The graphs of $f_{I\tau y}$ are scaled by a factor of $1/\lambda$ for the comparison with f_{Ay}. The supply ratio w tends to be negative in cases with $T_L = 0$ or J-PSMF, which means that the passivity was lost in these cases.

experimenter. When the phase-lead compensator was used ($T_L > 0$), it was easier to produce the periodic motion, but as can be seen in Fig. 11(d)(e), the results of J-PSMF were rather unstable, exhibiting the large negative values of w and the perturbed periodicity of the motion.

With M-PSMF and the phase-lead compensator ($T_L > 0$), it was easy to continue the periodic motion. Negative values of w are seen in Fig. 11(e), though they are not as large as those in the other cases. The experimenter, however, did not feel active perturbation from the master robot. Relatively small negative w values in Fig. 11(e) may be attributed to the non-collocation between the force sensor and the angle sensors, which were separated by the compliant transmissions.

One can see that $f_{I\tau y}$ was much smaller than λf_{Ay}, which means that the force at this frequency (approximately 3 Hz) was attenuated by the filter. Effects of the filter on lower-frequency components will be discussed based on the results of the next Experiment III.

D. Experiment III: 6-DOF Motion and External Contacts with M-PSMF

In this set of experiments, all the six joints of each robot were employed and the slave robot gained contact with an external environment. A short wooden shelf was placed in front of the slave robot and was used as the environment. The experimenter moved the master robot so that the slave robot should (i) draw a circular path in the air, (ii) move downward to gain contact with the environment, (iii) push the environment for three times, and (iv) move upward and again draw a circular path in the air. Fig. 12 shows the slave robot in contact with the environment.

The force scaling factor was chosen as $\lambda = 25$. With this λ value, J-PSMF or $T_L = 0$ produced unstable or oscillatory behavior of the system, and thus the aforementioned manipulation (drawing a circular path and making contact with an environment) cannot be realized. With higher λ values, the system also tended to be oscillatory. We therefore report here the results of only the case with M-PSMF, $T_L > 0$ and $\lambda = 25$.

The results are shown in Fig 13. As can be seen in this figure, the whole process was realized without losing the stability or producing significant oscillation. The filtered force

Fig. 12. Experiment III: slave robot in contact with the external environment (a wooden shelf).

($f_{I\tau y}$, $f_{I\tau z}$) was smaller than the scaled original force (λf_{Ay}, λf_{Az}) during the fast motion ($t < 2$ s and $t > 8$ s), but it was close to the scaled original force during the contact periods (three separated periods within $t \in [3\text{ s}, 8\text{ s}]$). From these results, one can say that at least the static transparency is achieved though high-frequency components (above 2 Hz) of the force are attenuated. Considering that the bandwidth of human voluntary motion is approximately up to 5 Hz (see, e.g., [42], [43]), one may say that the bandwidth of the filter should be broadened without losing the noise reduction capability to achieve a better realization of the human manual skills through the MS system. This point should be noted in the future study.

V. Conclusions

This paper has proposed a nonlinear noise reduction filter based on sliding mode. We also have proposed its combined application with the conventional linear phase-lead compensator to enhance the stability of force-projecting MS systems. A motivation of the use of phase-lead compensation in force-projecting and force-reflecting MS systems has been discussed based on the linear control theory. Through a numerical analysis on the proposed filter, it has been shown that the filter produces smaller phase lag than the linear low-pass filters. The effectiveness of the new filter combined with the phase-lead compensator has been validated by experiments employing a pair of industrial manipulators. As our primary focus has been placed on MS systems for force scaling instead of telepresence, the effect of communication latency has been left outside the scope of this paper.

An important issue remaining is that, as can be seen in Fig. 11(f) and Fig. 13, the filter attenuates the frequency components above 2 or 3 Hz of the force. In order to broaden the bandwidth at least up to 5 Hz (considering the characteristics of the human voluntary movements), a further optimization of the filter performance will be necessary. Besides that, inconsistencies between the numerical results and experimental observations are also subject to future study. For example, section IV-C has pointed out that the effects of the H value are not as predicted by the frequency-domain analysis in section III-C. A more detailed analysis, not only in the frequency domain but also in the time domain, will be needed.

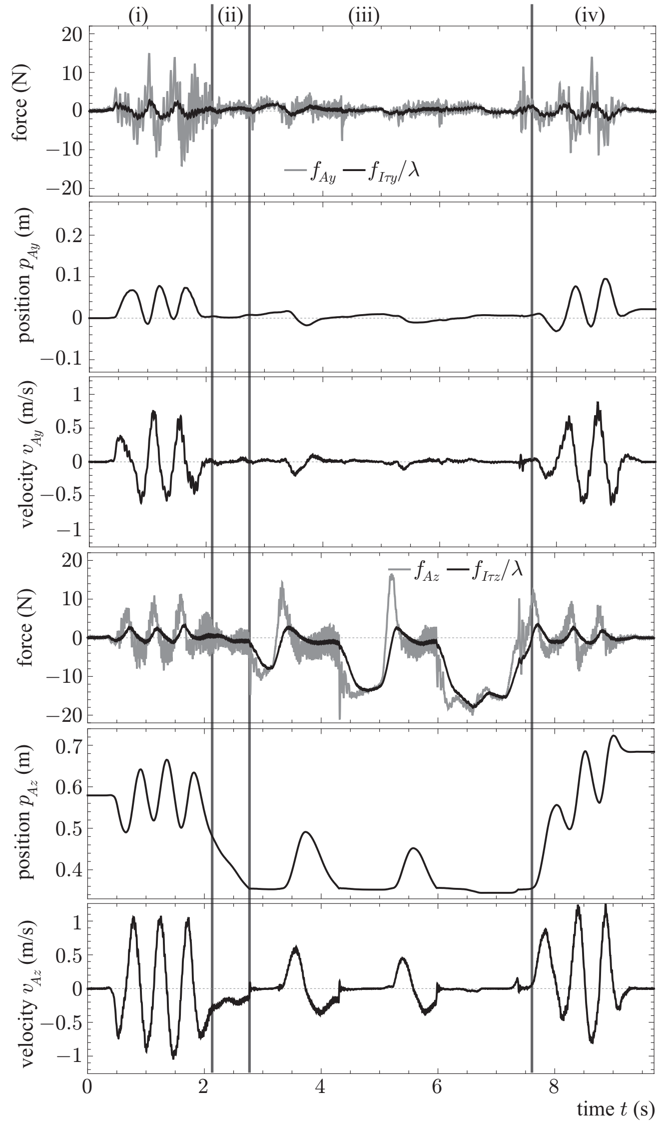

Fig. 13. Experiment III: the master robot's end-effector was (i) grasped and shaken in the air, (ii) moved down to gain contact with an environment, (iii) pushed to the environment for three times, and (iv) moved upward and again shaken in the air. The M-PSMF was used and the parameters were chosen as: $\lambda = 25$, $T_L = 0.02$ s, $F = 4 \times 10^3$ N/s^2, $H = 300$.

Another issue in the implementation is the singularity management of the master robot. In the experiments presented in this paper, the master robot and the slave robot had the identical kinematic structure, but it will not be the case for practical applications. In such cases, the master robot may need careful mechanical design so that it does not fall into singular configurations. It is worth pointing out that, on the other hand, the slave robot does not need such considerations for its design.

Though the experimental validation in this paper is limited to a force-projecting MS system, the method would be applicable to conventional force-reflecting MS systems to enhance the stability. A broader bandwidth of the filter may be needed for such applications, though a higher force-scaling factor enabled by the enhanced stability may contribute a better transparency, i.e., the operator's perception of the remote site.

APPENDIX
STABILITY ANALYSIS OF M-PSMF

This section provides a proof of Theorem 1. To this end, let us rewrite the state-space representation of the new filter (23) as follows:

$$\dot{\xi} \in \Psi(\xi, e) \tag{29}$$

where

$$\xi \triangleq [\eta, v]^T \tag{30}$$

$$e \triangleq [\dot{u}, \ddot{u}]^T \tag{31}$$

$$\Psi(\xi, e) \triangleq \begin{bmatrix} (1-L)v \\ -\ddot{u} \end{bmatrix} - \begin{bmatrix} |v+\dot{u}| \\ G \end{bmatrix} (\mathrm{sgn}(\eta) + L\mathrm{sgn}(v)) \tag{32}$$

$$\eta \triangleq (1-L)(x_1 - u) + |x_2|x_2/(2G) \tag{33}$$

$$v \triangleq x_2 - \dot{u} \tag{34}$$

$$G \triangleq (H+1)F/2 \tag{35}$$

$$L \triangleq (H-1)/(H+1) < 1. \tag{36}$$

Here, we used the fact that $\mathrm{sgn}(\sigma) = \mathrm{sgn}(\eta)$. Note that $\Psi(\xi)$ is a set-valued function. For the convenience of the following discussion, let us define the closed interval $\mathcal{B} \triangleq [-1, 1] \subset \mathbb{R}$ and the zero vector $\mathcal{O} \triangleq [0, 0]^T \in \mathbb{R}^2$. The Filippov solution [44], [45] of the differential inclusion (29) is a function $\xi(t)$ of the time t that satisfies (29) for almost every $t \in \mathbb{R}$.

Based on the notation introduced above, let us rewrite Theorem 1 as follows:

Theorem 2. *For the system (29), assume that there exist positive constants P and Q that satisfy the following conditions for all $t > t_0$:*

$$|\dot{u}| < P, \text{ and } |\ddot{u}| < Q < \min(LG, (1-L)G). \tag{37}$$

Then, the system (29) is globally uniformly ultimately bounded and the ultimate bound is the following compact set:

$$\mathcal{A} \triangleq \left\{ \xi \in \mathbb{R}^2 \;\middle|\; \eta = 0 \wedge |v| \le \frac{PQ}{(1-L)G - Q} \right\}. \tag{38}$$

The following discussion is to prove Theorem 2. First, let us present the following useful lemma:

Lemma 1. *In the system (29), $\eta \ne 0$ is satisfied for almost all $t \in \mathbb{R}$ at which $\xi \in \mathcal{N}(\dot{u})$ where*

$$\mathcal{N}(\dot{u}) \triangleq \left\{ \xi \in \mathbb{R}^2 \;\middle|\; \frac{1+L}{1-L}|v + \dot{u}| < |v| \right\}. \tag{39}$$

Proof of Lemma 1: In the system (29), $\eta = 0$ and $\dot{\eta} = 0$ can be satisfied only if

$$0 \in (1-L)v - |v + \dot{u}| (\mathcal{B} + L\mathrm{sgn}(v)) \tag{40}$$

is satisfied. When $v = 0$, (40) always holds true. Otherwise, (40) is equivalent to

$$\begin{aligned} -(1 - L\mathrm{sgn}(v))|v + \dot{u}| &\le (1-L)v \\ &\le (1 + L\mathrm{sgn}(v))|v + \dot{u}|. \end{aligned} \tag{41}$$

Through a tedious but straightforward derivation, one can obtain the necessary and sufficient condition of (40) as follows:

$$|v| \le \frac{1+L}{1-L}|v + \dot{u}|, \tag{42}$$

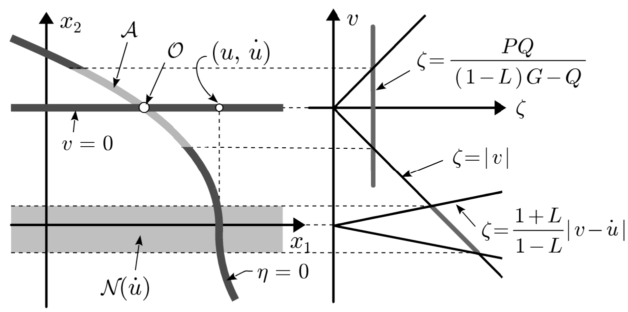

Fig. 14. The set $\mathcal{N}(\dot{u})$ and the terminal invariant set $\mathcal{A}$ in the state space. (The variable ζ is defined here only for the convenience of illustration.)

which is equivalent to $\xi \notin \mathcal{N}(\dot{u})$. Considering that η is an absolutely continuous function of t, one can see that $\eta = 0$ is satisfied only at zero-length time instants when $\xi \in \mathcal{N}(\dot{u})$ holds true because $\dot{\eta} = 0$ cannot hold true at such instants. In other words, $\eta \ne 0$ is satisfied at almost all $t \in \mathbb{R}$ if $\xi \in \mathcal{N}(\dot{u})$ is satisfied. ■

The inequality (42) is the condition of the existence of the sliding mode on the surface $\eta = 0$. That is, the state is captured on the surface $\eta = 0$ outside the region $\mathcal{N}(\dot{u})$, but penetrates the surface $\eta = 0$ in the region $\mathcal{N}(\dot{u})$. Fig. 14 illustrates the set $\mathcal{N}(\dot{u})$ and the set $\mathcal{A}$. The terminal invariant set $\mathcal{A}$ is a portion of the surface $\eta = 0$ around the intersection with the line $v = 0$, and always lays outside the region $\mathcal{N}(\dot{u})$ when (37) is satisfied. It is also easy to see that the set $\mathcal{A}$ has the following property:

Remark 1. *The set $\mathcal{A}$ reduces to $\mathcal{A} = \mathcal{O}$ if and only if $(P = 0 \wedge Q < (1-L)G) \vee Q = 0$.*

Now we are in position to provide a proof of Theorem 2.

Proof of Theorem 2: Let us define the following Lyapunov function candidate:

$$V(\xi) \triangleq \frac{|\eta|}{1-L} + \frac{v^2}{2G}. \tag{43}$$

The function $V(\xi)$ is zero at $\xi = \mathcal{O}$. The generalized gradient [45] of $V(\xi)$ can be obtained as follows:

$$\partial V(\xi) = \begin{bmatrix} \dfrac{\mathrm{sgn}(\eta)}{1-L} & \dfrac{v}{G} \end{bmatrix}^T. \tag{44}$$

Because $\xi(t)$ is absolutely continuous with respect to t, we can see that $V(\xi(t))$ is also absolutely continuous with respect to t. This implies that $\dot{V}(\xi(t))$ exists for almost all $t \in \mathbb{R}$, and that the following is satisfied [46]:[7]

$$\dot{V}(\xi) \overset{\text{a.a.}t}{\in} \dot{\overline{V}}(\xi) \triangleq \bigcup_{\psi \in \Psi(\xi)} \bigcap_{\phi \in \partial V(\xi)} \psi^T \phi \tag{45}$$

where "a.a." means "almost all." Here, $\dot{\overline{V}}(\xi)$ is referred to as a set-valued derivative [46] of $V(\xi)$ with respect to (29).

[7] Prior to Bacciotti and Ceragioli [46], Shevitz and Paden [47] presented another definition of a set-valued derivative $\dot{\tilde{V}}(\xi) \triangleq \cap_{\phi \in \partial V(\xi)} \cup_{\psi \in \Psi(\xi)} \psi^T \phi$, where the order of $\cap$ and $\cup$ is opposite to $\dot{\overline{V}}$ in (45). It has been pointed out [46] that $\dot{\overline{V}} \subset \dot{\tilde{V}}$, which means that $\dot{\overline{V}}$ is more precise than $\dot{\tilde{V}}$.

Now, let us investigate the details of $\dot{\overline{V}}(\xi)$. When $\eta \neq 0$, $\dot{\overline{V}}(\xi)$ can be rewritten as follows:

$$\begin{aligned}\dot{\overline{V}}(\xi) &= v\left(\mathrm{sgn}(\eta) - \frac{\ddot{u}}{G}\right) - v\left(\mathrm{sgn}(\eta) + L\mathrm{sgn}(v)\right) \\ &\quad - \frac{\mathrm{sgn}(\eta)|v+\dot{u}|}{1-L}\left(\mathrm{sgn}(\eta) + L\mathrm{sgn}(v)\right) \\ &= \begin{cases} -\dfrac{v\ddot{u}}{G} - L|v| - |v+\dot{u}|\dfrac{1+L\mathrm{sgn}(\eta v)}{1-L} & \\ & \text{if } \eta \neq 0 \wedge v \neq 0 \\ \left[-\dfrac{1+L}{1-L}|\dot{u}|, -|\dot{u}|\right] & \text{if } \eta \neq 0 \wedge v = 0. \end{cases} \end{aligned} \tag{46}$$

Meanwhile, when $\eta = 0$, $\dot{\overline{V}}(\xi)$ can be rewritten as follows:

$$\begin{aligned}\dot{\overline{V}}(\xi) &= \bigcup_{\theta\in\mathcal{B}}\bigcap_{\gamma\in\mathcal{B}}\left(v\left(\gamma - \frac{\ddot{u}}{G}\right) - v\left(\theta + L\mathrm{sgn}(v)\right)\right. \\ &\quad \left. - \frac{\gamma|v+\dot{u}|}{1-L}\left(\theta + L\mathrm{sgn}(v)\right)\right) \\ &= -\frac{v\ddot{u}}{G} - L|v| + \bigcup_{\theta\in\mathcal{B}}\Gamma(v,\theta) \end{aligned} \tag{47}$$

where

$$\begin{aligned}\Gamma(v,\theta) &\triangleq -\theta v + \bigcap_{\gamma\in\mathcal{B}}\gamma\left(v - \frac{|v+\dot{u}|}{1-L}\left(\theta + L\mathrm{sgn}(v)\right)\right) \\ &= \begin{cases} -\theta v & \text{if } 0 \in v - \dfrac{|v+\dot{u}|}{1-L}\left(\theta + L\mathrm{sgn}(v)\right) \\ \emptyset & \text{otherwise.} \end{cases}\end{aligned} \tag{48}$$

One can easily see that $\theta \in \mathcal{B}$ satisfying $\Gamma(v,\theta) \neq \emptyset$ exists only when $\xi \in \mathcal{N}(\dot{u})$. Therefore, $\dot{\overline{V}}(\xi)$ under the condition of $\eta = 0$ can be obtained as follows:

$$\dot{\overline{V}}(\xi) = \begin{cases} \emptyset & \text{if } \eta = 0 \wedge \xi \in \mathcal{N}(\dot{u}) \\ -\dfrac{v\ddot{u}}{G} - \dfrac{v^2(1-L)}{|v+\dot{u}|} & \\ & \text{if } \eta = 0 \wedge \xi \notin \mathcal{N}(\dot{u}) \wedge v + \dot{u} \neq 0 \\ 0 & \text{if } \eta = 0 \wedge v = 0 \wedge \dot{u} = 0. \end{cases} \tag{49}$$

Here, note that the condition $v = 0 \wedge \dot{u} = 0$ is interchangeable with $\xi \notin \mathcal{N}(\dot{u}) \wedge v + \dot{u} = 0$. In addition, one can see that $\dot{\overline{V}}(\xi) \neq \emptyset$ is satisfied for almost all $t \in \mathbb{R}$ from Lemma 1, which implies that $\eta = 0 \wedge \xi \in \mathcal{N}(\dot{u})$ cannot hold true for a time period of non-zero length. This fact is consistent with the property (45) of the set-valued derivative.

Now, we apply the fact

$$\max(0, |v| - P) < |v + \dot{u}| < |v| + P \tag{50}$$

to (46) and (49) to obtain the upperbound of $\dot{\overline{V}}(\xi)$. From (46), when $\eta \neq 0$ and $v \neq 0$,

$$\begin{aligned}\dot{\overline{V}}(\xi) &\leq -|v|\left(\frac{LG-Q}{G}\right) - \frac{1+L\mathrm{sgn}(\eta v)}{1-L}\max(0,|v|-P) \\ &< 0\end{aligned} \tag{51}$$

is obtained, and one can see that $\dot{\overline{V}}(\xi) \subset (-\infty, 0]$ if $\eta \neq 0$. In addition, $\dot{\overline{V}}(\xi) \ni 0$ may happen only when $v = 0$. The state-space representation (29) implies that $\dot{v} = 0$ cannot be satisfied if $\eta \neq 0$ under the condition (37). This means that $\dot{\overline{V}}(\xi) \ni \dot{V}(\xi) < 0$ is satisfied for almost all t when $\eta \neq 0$.

From (49), when $\eta = 0 \wedge \xi \notin \mathcal{N}(\dot{u}) \wedge v + \dot{u} \neq 0$, one can obtain the following:

$$\begin{aligned}\dot{\overline{V}}(\xi) &\leq \frac{|v|Q}{G} - \frac{|v|^2(1-L)}{|v|+P} \\ &= -\frac{((1-L)G-Q)|v|}{G(|v|+P)}\left(|v| - \frac{PQ}{(1-L)G-Q}\right).\end{aligned} \tag{52}$$

When $\xi \in \mathcal{A}$, the right-hand side of (52) is positive. Considering (52) and $\dot{\overline{V}}(\xi)$ in all other conditions, one can see that $\dot{V}(\xi) \in \dot{\overline{V}}(\xi) \subset (-\infty, 0)$ is satisfied for almost all t except when $\xi \in \mathcal{A}$. Because $\mathcal{A}$ is a compact set including the origin $\mathcal{O}$ where $V(\xi) = 0$, one can see that, as long as (37) is satisfied, the state ξ is attracted to $\mathcal{A}$, and after it reaches to $\mathcal{A}$, it does not deviate from $\mathcal{A}$. ■

REFERENCES

[1] D. A. Lawrence, "Stability and transparency in bilateral teleoperation," *IEEE Transactions on Robotics and Automation*, vol. 9, no. 5, pp. 624–637, 1993.

[2] H. Y. K. Lau and L. C. C. Wai, "Implementation of position-force and position-position teleoperator controllers with cable-driven mechanisms," *Robotics and Computer-Integrated Manufacturing*, vol. 21, pp. 145–152, 2005.

[3] M. Mahvash and A. M. Okamura, "Enhancing transparency of a position-exchange teleoperator," in *Proceedings of Second Joint EuroHaptics Conference and Symposium on Haptic Interfaces for Virtual Environment and Teleoperator Systems (WHC'07)*, 2007, pp. 470–475.

[4] J. Artigas, J.-H. Ryu, and C. Preusche, "Time domain passivity control for position-position teleoperation architectures," *Presence*, vol. 19, no. 5, pp. 482–497, 2010.

[5] Y. Yokokohji and T. Yoshikawa, "Bilateral control of master-slave manipulators for ideal kinesthetic coupling — formulation and experiment," *IEEE Transactions on Robotics and Automation*, vol. 10, no. 5, pp. 605–610, 1994.

[6] E. B. Vander Poorten, Y. Yokokohji, and T. Yoshikawa, "Stability analysis and robust control for fixed-scale teleoperation," *Advanced Robotics*, vol. 20, no. 6, pp. 681–706, 2006.

[7] T. L. Brooks, "Telerobotic response requirements," *Proceedings of 1990 IEEE International Conference on Systems, Man and Cybernetics*, pp. 113–120, 1990.

[8] K. Hashtrudi-Zaad and S. E. Salcudean, "Analysis of control architectures for teleoperation systems with impedance/admittance master and slave manipulators," *International Journal of Robotics Research*, vol. 20, no. 6, pp. 419–445, 2001.

[9] J. Kim, P. H. Chang, and H. W. Park, "Two-channel transparency-optimized control architectures in bilateral teleoperation with time delay," *IEEE Transactions on Control Systems Technology*, vol. 21, no. 1, pp. 40–51, 2013.

[10] H. Wang, K. H. Low, and M. Y. Wang, "A bilateral teleoperation controller considering the transition between the free space motion and the constrained motion," *Robotica*, vol. 26, no. 6, pp. 781–790, 2008.

[11] B. Hannaford, L. Wood, D. A. McAffee, and H. Zak, "Performance evaluation of a six-axis generalized force-reflecting teleoperator," *IEEE Transactions on Systems, Man and Cybernetics*, vol. 21, no. 3, pp. 620–633, 1991.

[12] R. W. Daniel and P. R. McAree, "Fundamental limits of performance for force reflecting teleoperation," *International Journal of Robotics Research*, vol. 17, no. 8, pp. 811–830, 1998.

[13] A. Tobergte and A. Albu-Schäffer, "Direct force reflecting teleoperation with a flexible joint robot," in *Proceedings of the 2012 IEEE International Conference on Robotics and Automation*, 2012, pp. 4280–4287.

[14] K. Kanaoka, "Force projection type bilateral control for power-amplifying master-slave systems," in *Proceedings of the 13th Annual Conference of Robotics Society of Japan*, 2009, pp. 3C1–06, (in Japanese).

[15] ——, "Master/slave system and method for controlling same," WIPO Patent Application WO 2011/115 287 A1, 2011.

[16] E. Naerum and B. Hannaford, "Global transparency analysis of the Lawrence teleoperator architecture," *Proceedings of the 2009 IEEE International Conference on Robotics and Automation*, pp. 4344–4349, 2009.
[17] K. J. Kuchenbecker and G. Niemeyer, "Induced master motion in force-reflecting teleoperation," *Transactions of ASME: Journal of Dynamic Systems, Measurement, and Control*, vol. 128, no. 4, pp. 808–810, 2006.
[18] P. Shull and G. Niemeyer, "Force and position scaling limits for stability in force reflecting teleoperation," in *Proceedings of the ASME 2008 Dynamic Systems and Control Conference*, 2008, pp. 607–614.
[19] B. Willaert, B. Corteville, D. Reynaerts, H. Van Brussel, and E. B. Vander Poorten, "A mechatronic analysis of the classical position-force controller based on bounded environment passivity," *International Journal of Robotics Research*, vol. 30, no. 4, pp. 444–462, 2011.
[20] S. Jin, R. Kikuuwe, and M. Yamamoto, "Real-time quadratic sliding mode filter for removing noise," *Advanced Robotics*, vol. 26, no. 8-9, pp. 877–896, 2012.
[21] ——, "Parameter selection guidelines for a parabolic sliding mode filter based on frequency and time domain characteristics," *Journal of Control Science and Engineering*, vol. 2012, Article ID 923679, 2012.
[22] T. Imaida, Y. Yokokohji, T. Doi, M. Oda, and T. Yoshikawa, "Ground-space bilateral teleoperation of ETS-VII robot arm by direct bilateral coupling under 7-s time delay condition," *IEEE Transactions on Robotics and Automation*, vol. 20, no. 3, pp. 499–511, 2004.
[23] W. S. Kim, B. Hannaford, and A. K. Bejczy, "Force-reflection and shared compliant control in operating telemanipulators with time delay," *IEEE Transactions on Robotics and Automation*, vol. 8, no. 2, pp. 176–185, 1992.
[24] W. S. Kim, "Developments of new force reflecting control schemes and an application to a teleoperation training simulator," in *Proceedings of the 1992 IEEE International Conference on Robotics and Automation*, 1992, pp. 1412–1419.
[25] H. P. Qian and J. De Schutter, "Introducing active linear and nonlinear damping to enable stable high gain force control in case of stiff contact," in *Proceedings of the 1992 IEEE International Conference on Robotics and Automation*, 1992, pp. 1375–1380.
[26] Y. Xu, J. M. Hollerbach, and D. Ma, "A nonlinear PD controller for force and contact transient control," *IEEE Control Systems*, vol. 15, no. 1, pp. 15–21, 1995.
[27] C. Natale, R. Koeppe, and G. Hirzinger, "A systematic design procedure of force controllers for industrial robots," *IEEE/ASME Transactions on Mechatronics*, vol. 5, no. 2, pp. 122–131, 2000.
[28] M. Boukhnifer and A. Ferreira, "H_∞ loop shaping bilateral controller for a two-fingered tele-micromanipulation system," *IEEE Transactions on Control Systems Technology*, vol. 15, no. 5, pp. 891–905, 2007.
[29] J. J. Abbott and A. M. Okamura, "Pseudo-admittance bilateral telemanipulation with guidance virtual fixtures," *International Journal of Robotics Research*, vol. 26, no. 8, pp. 865–884, 2007.
[30] A. Peer, B. Stanczyk, and M. Buss, "Haptic telemanipulation with dissimilar kinematics," in *Proceedings of the 2005 IEEE/RSJ International Conference on Intelligent Robots and Systems*, 2005, pp. 2483–2488.
[31] A. Peer and M. Buss, "A new admittance-type haptic interface for bimanual manipulations," *IEEE/ASME Transactions on Mechatronics*, vol. 13, no. 4, pp. 416–428, 2008.
[32] J. Park and O. Khatib, "A haptic teleoperation approach based on contact force control," *International Journal of Robotics Research*, vol. 25, no. 5-6, pp. 575–591, 2006.
[33] R. Kikuuwe, "A sliding-mode-like position controller for admittance control with bounded actuator force," *IEEE/ASME Transactions on Mechatronics*, vol. 19, no. 5, pp. 1489–1500, 2014.
[34] G. V. Smirnov, *Introduction to the Theory of Differential Inclusions*. Providence, Rhode Islands, USA: American Mathematical Society, 2002.
[35] S. Jin, R. Kikuuwe, and M. Yamamoto, "Improving velocity feedback for position control by using a discrete-time sliding mode filtering with adaptive windowing," *Advanced Robotics*, vol. 28, no. 14, pp. 943–953, 2014.
[36] A. Levant, "Principles of 2-sliding mode design," *Automatica*, vol. 43, no. 4, pp. 576–586, 2007.
[37] T. Emaru and T. Tsuchiya, "Research on estimating smoothed value and differential value by using sliding mode system," *IEEE Transactions on Robotics and Automation*, vol. 19, no. 3, pp. 391–402, 2003.
[38] J.-Q. Han and W. Wang, "Nonlinear tracking-differentiator," *Journal of System Science and Mathematical Science*, vol. 14, no. 2, pp. 177–183, 1994, (in Chinese).
[39] J.-J. E. Slotine and W. Li, *Applied Nonlinear Control*. Prentice Hall, 1990.
[40] D. Sun, F. Naghdy, and H. Du, "Application of wave-variable control to bilateral teleoperation systems: A survey," *Annual Reviews in Control*, vol. 38, no. 1, pp. 12–31, 2014.
[41] I. G. Polushin, P. X. Liu, and C.-H. Lung, "A force-reflection algorithm for improved transparency in bilateral teleoperation with communication delay," *IEEE/ASME Transactions on Mechatronics*, vol. 12, no. 3, pp. 361–374, 2007.
[42] K. A. Mann, F. W. Wernere, and A. K. Palmer, "Frequency spectrum analysis of wrist motion for activities of daily living," *Journal of Orthopaedic Research*, vol. 7, no. 2, pp. 304–306, 1989.
[43] J. M. Hollerbach, "An oscillation theory of handwriting," *Biological Cybernetics*, vol. 39, no. 2, pp. 139–156, 1981.
[44] A. F. Filippov, *Differential Equations with Discontinuous Righthand Sides*. Kluwer Academic Publishers, 1988.
[45] J. Cortés, "Discontinuous dynamical systems," *IEEE Control Systems*, vol. 28, no. 3, pp. 36–73, 2008.
[46] A. Bacciotti and F. Ceragioli, "Stability and stabilization of discontinuous systems and nonsmooth Lyapunov functions," *ESAIM: Control, Optimisation and Calculus of Variations*, vol. 4, pp. 361–376, 1999.
[47] D. Shevitz and B. Paden, "Lyapunov stability theory of nonsmooth systems," *IEEE Transactions on Automatic Control*, vol. 39, no. 9, pp. 1910–1914, 1994.

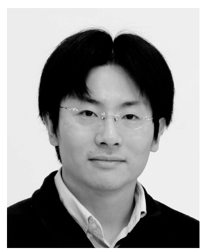

Ryo Kikuuwe (S'02-M'03) received the B.S., M.S., and Ph.D.(Eng.) degrees from Kyoto University, Kyoto, Japan, in 1998, 2000, and 2003, respectively, all in mechanical engineering. From 2003 to 2007, he was an Endowed-Chair Research Associate at Nagoya Institute of Technology, Nagoya, Japan. Since 2007, he has been an Associate Professor at the Department of Mechanical Engineering, Kyushu University, Fukuoka, Japan. From 2014 to 2015, he was a Visiting Researcher at INRIA Grenoble Rhône-Alpes, France.

His research interests include physical human-robot interaction, real-time simulation for physics-based animation, and engineering applications of differential inclusions.

Prof. Kikuuwe is a member of the Robotics Society of Japan, Japan Society of Mechanical Engineers, Society of Instrument and Control Engineers (Japan), and Virtual Reality Society of Japan. He received the Best Paper Award of Advanced Robotics in 2013, and the Young Investigator Excellence Award from the Robotics Society of Japan in 2005.

Katsuya Kanaoka received the B.S. and M.S. degrees in chemical engineering and the Ph.D. degree in mechanical engineering from Kyoto University, Kyoto, Japan, in 1995, 1997, and 2002, respectively.

He was a Research Associate from 2002 to 2003 and a Lecturer from 2003 to 2008 with Ritsumeikan University, Kusatsu, Japan. Since 2007, he has been a CEO & CTO of Man-Machine Synergy Effectors Inc., Kusatsu, Japan. Simultaneously, since 2008, he has been a Chair Professor with Ritsumeikan University.

Tomohiro Kumon received the B.E. degree from Kyushu University, Fukuoka, Japan, in 2011 in mechanical engineering. At the time of writing this paper, he was with the Department of Mechanical Engineering, Kyushu University, Fukuoka, Japan, where he received the M.E. degree in 2013 in mechanical engineering.

He is currently with KYB Co. Ltd., Tokyo, Japan.

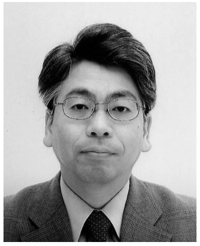

Motoji Yamamoto (M'02) received the B.E., M.S., and Dr. Eng. degrees from Kyushu University, Fukuoka, Japan, in 1985, 1987, and 1990, respectively, all in mechanical engineering.

In 1990, he joined the Department of Intelligent Machinery and Systems, Kyushu University as a Lecturer, and was promoted to an Associate Professor and a Professor in 1992 and 2005, respectively. Currently, he is with the Department of Mechanical Engineering, Kyushu University. His research interests include field and service robots, parallel wire mechanisms, human care and medical robots.